ACS APPLIED MATERIALS & INTERFACES

Research Article

www.acsami.org

Synthesis of Fullerene−, Carbon Nanotube−, and Graphene−TiO_2 Nanocomposite Photocatalysts for Selective Oxidation: A Comparative Study

Min-Quan Yang, Nan Zhang, and Yi-Jun Xu*

State Key Laboratory Breeding Base of Photocatalysis, College of Chemistry and Chemical Engineering, Fuzhou University, Fuzhou, 350002, P.R. China

Supporting Information

ABSTRACT: A series of TiO_2−graphene (GR), −carbon nanotube (CNT), and −fullerene (C_{60}) nanocomposite photocatalysts with different weight addition ratios of carbon contents are synthesized via a combination of sol−gel and hydrothermal methods. Their structures and properties are determined by the X-ray diffraction (XRD), UV−vis diffuse reflectance spectra (DRS), transmission electron microscopy (TEM), nitrogen adsorption−desorption, and photoelectrochemical measurements. Photocatalytic selective oxidation of benzyl alcohol to benzaldehyde is employed as a model reaction to evaluate the photocatalytic activity of the TiO_2−carbon (GR, CNT, and C_{60}) nanocomposites under visible light irradiation. The results reveal that incorporating TiO_2 with carbon materials can extend the adsorption edge of all the TiO_2−carbon nanocomposites to the visible light region. For TiO_2−GR, TiO_2−CNT, and TiO_2−C_{60} nanocomposites, the photocatalytic activities of the composites with optimum ratios, TiO_2−0.1% GR, TiO_2−0.5% CNT, and TiO_2−1.0% C_{60}, are very close to each other along with the irradiation time. Furthermore, the underlying reaction mechanism for the photocatalytic selective oxidation of benzyl alcohol to benzaldehyde over TiO_2−carbon nanocomposites has been explored using different radical scavenger techniques, suggesting that TiO_2−carbon photocatalysts follow the analogous oxidation mechanism toward selective oxidation of benzyl alcohol. The addition of different carbon materials has no significant influence on the crystal phase, particle size, and the morphology of TiO_2. Therefore, it can be concluded, at least for nanocomposites of TiO_2−carbon (GR, CNT, and C_{60}) obtained by the present approach, that there is no much difference in essence on affecting the photocatalytic performance of semiconductor TiO_2 among these three different carbon allotropes, GR, CNT, and C_{60}. Our findings point to the importance of a comparative study of semiconductor−carbon photocatalysts on drawing a relatively objective conclusion rather than separately emphasizing the unique role of GR and joining the graphene gold rush.

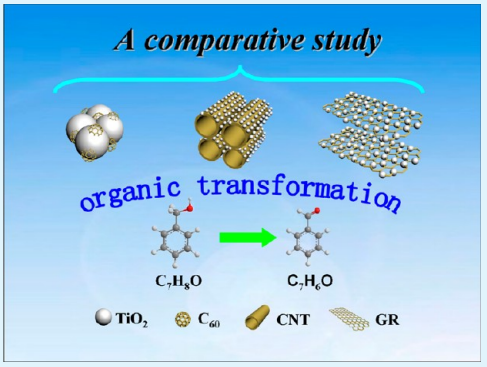

KEYWORDS: *TiO_2, graphene, fullerene, carbon nanotube, visible light irradiation, selective oxidation*

1. INTRODUCTION

Graphene (GR), as a new allotrope of carbon, has attracted an enormous amount of interest from both theoretical and experimental scientists since its discovery in 2004 by Geim and co-workers.[1] Due to its exceptional properties, such as excellent electron mobility,[2,3] theoretically large surface area of ~2600 m^2/g,[4] high thermal conductivity of ~5000 W m^{-1} K^{-1}, and optical transparency,[5,6] GR projects as a rapidly rising star on the horizon of materials science and condensed matter physics.[7,8] Thus far, GR−based nanocomposites have been widely explored in a myriad of fields, including biosensors, nanoelectronics, intercalation materials, drug delivery, catalysis, supercapacitors, and polymer composites.[9−22] With regard to the domain of photocatalysis, GR, the thinnest and the strongest material ever known in the universe,[9] also catches the eyes of researchers in this field and, indeed, promotes great interest to synthesize GR−semiconductor nanocomposites as photocatalysts for target applications.[14,20,21,23−42]

Researchers have synthesized multifarious, versatile GR−semiconductor nanocomposites as photocatalysts for degradation of pollutants (e.g., dyes, bacteria, and volatile organic pollutants),[25−31] selective organic transformations for synthesis of fine chemicals,[32−36] and water splitting to H_2.[37−44] What is notable from the reported literature is that nearly all of the research works are inclined to highlight that the enhanced photocatalytic activity of GR−semiconductor nanocomposites is aroused from the addition of GR having exceptional properties. But if we dispassionately look back at the development history of the carbon family, this situation seems to have ever happened, when zero-dimension fullerene (C_{60}) and one-dimensional carbon nanotube (CNT) first appeared,[45,46] which we praised generously with kind words,

Received: December 5, 2012
Accepted: January 16, 2013
Published: January 16, 2013

too. That is, the abundant C_{60}–semiconductor and CNT–semiconductor nanomaterials with various morphologies as photocatalysts have already been reported,[47−58] and it has been well demonstrated that the addition of fullerene and carbon nanotubes is able to improve the photocatalytic performance of semiconductors, such as TiO_2,[49−51,54,59] very much similar to their allotrope GR. If we compare those C_{60}–semiconductor and CNT–semiconductor photocatalysts with their counterparts of GR–semiconductor, the following remarks can be easily found. The enhancement of photoactivity for all of the semiconductor–carbon (C_{60}, CNT, and GR) nanocomposites is ascribed to the fact that incorporation of carbon contents into the matrix of semiconductors will increase the adsorptivity, the absorption capability in the visible light region, and the life span of photoexcited electron–hole pairs. In particular, most research works state that C_{60}, CNT, and GR all can act as an electron reservoir to trap photoexcited electrons from semiconductors, thereby improving the life span of electron–hole pairs, which is always regarded as the most important factor contributing to the enhancement of photoactivity of semiconductor–carbon (C_{60}, CNT, and GR) nanocomposites.[27,32,33,37,47−49,53] Thus, these three carbon allotropes of C_{60}, CNT, and GR in the carbon family seem much similar in the aspect of improving photocatalytic performance of semiconductors. Furthermore, noting that GR is a two-dimensional sheet of sp^2 hybridized carbon,[15,60] its unique extended honeycomb network can be viewed as a basic building block for other carbon allotropes with different dimensionalities, including the wrapped zero-dimension buckyballs (fullerene) and the rolled one-dimension carbon nanotubes (CNTs).[7,10]

Thus, it is natural to raise such fundamental questions as the following. Since C_{60}, CNT, and GR have many similar structure and electronic properties in common, are they similar in improving the photocatalytic performance of semiconductors when we use them to assemble carbon–semiconductor composite photocatalysts? Without a basic comparison study between composite photocatalysts of GR–semiconductor, CNT–semiconductor, and C_{60}–semiconductor, are we rational to claim that the enhancement of photoactivity of GR–semiconductor is due to the unique and excellent electron conductivity of GR which prolongs the life span of photoexcited electron–hole pairs significantly? In other words, do we give incomplete or exaggerated information on the contribution role of GR to enhance the semiconductor photocatalytic activity, as compared to its carbon allotropes, fullerene, and carbon nanotube?[25,26]

Bearing these questions in mind, an integrated and comparison study which is still lacking in this field has been carried out in this work. By taking the mostly studied TiO_2 semiconductor as an example, we have synthesized a series of TiO_2–carbon (C_{60}, CNT, and GR) composite photocatalysts with different weight addition ratios of carbon contents using the same sol–gel approach to guarantee the good interfacial contact between TiO_2 and carbon ingredients. The sol–gel processing is one of the most common methods to produce nanocomposite photocatalysts, and it allows compositional and microstructural tailoring through controlling the precursor chemistry and processing conditions;[61] the approach makes it possible to control a number of determining parameters of the final product such as homogeneity, purity, and microstructure (in particular porosity and surface area).[62] Furthermore, the sol–gel approach provides excellent chemical homogeneity and the possibility of deriving unique metastable structures at low reaction temperatures. Using photocatalytic selective oxidation of benzyl alcohol to benzaldehyde as a model reaction, the influences of the carbon types and their contents on photocatalytic activity are discussed. Our results demonstrate the significant influence of preparation methods on the photocatalytic performance of TiO_2–carbon composites, and GR can not manifest its unique role as compared to its carbon allotropes. It is hoped that our research work could promote the more objective understanding on the analogy and difference of these three carbon allotropes, graphene, fullerene, and carbon nanotube on the rational synthesis and photoactivity improvement of semiconductor–carbon composites, instead of joining the graphene gold rush.

2. EXPERIMENTAL SECTION

2.1. Preparation. *Materials.* Graphite powder, nitric acid (HNO_3, 65%), absolute ethanol (C_2H_6O), benzyl alcohol (C_7H_8O), benzaldehyde (C_7H_6O), ammonium oxalate ($(NH_4)_2C_2O_4{\cdot}H_2O$), and silver nitrate ($AgNO_3$) are analytical grade; *tert*-butyl alcohol ($C_4H_{10}O$), benzoquinone ($C_6H_4O_2$), and tetrabutyl titanate (Ti$(OC_4H_9)_4$), purity ≥ 98.0%) are chemical pure. All of the above chemicals were obtained from Sinopharm Chemical Reagent Co., Ltd. (Shanghai, China) and used as received without further purification. Benzotrifluoride (BTF, purity > 99%) was supplied by Alfa Aesar China Co., Ltd. (Tianjin, China). Carbon nanotubes were purchased from Shenzhen Nanotech Port Co., Ltd., China. High-purity C_{60} (99.9%) was obtained from Yongxin Chemical Reagent Company (Henan, China). Deionized (DI) water used in the synthesis was from local sources.

Synthesis. (a) Synthesis of Graphene Oxide (GO). Graphene oxide (GO) was synthesized from natural graphite powder by a modified Hummers' method, as also reported in our previous research works.[26,32,63]

(b) Treatment of Fullerenes (C_{60}) and Carbon Nanotubes (CNT). The purification and surface functionalization of C_{60} and CNTs were carried out before used for nanocomposites. A 50 mg portion of raw C_{60} was refluxed in 150 mL of concentrated nitric acid at 140 °C for 4 h. Then, the dark brown solid was collected by centrifugation and washed with DI water several times until pH = 7. After that, the product was dried at 60 °C in an oven. The CNTs used here were multiwalled carbon nanotubes, which were treated by the same procedure.

(c) Fabrication of TiO_2–Carbon (GR, CNT, C_{60}) Nanocomposites. The preparation of TiO_2–carbon nanocomposite photocatalysts is outlined as follows. The weight addition ratios of carbon are selected as 0.1%, 0.5%, 1%, 5%, 10%, and 20%. A certain amount of carbon materials was sonicated in a mixed solution of 9 mL ethanol and 18 mL DI water. The ultrasonic time should be long enough to ensure the thorough dispersion of carbon materials. Then, 1.7 mL tetrabutyl titanate (TBOT) was mixed with 9 mL ethanol and added dropwise to the above solution of carbon materials with magnetic stirring. After stirring for 3 h, the suspension was transferred into a 50 mL Teflon-lined autoclave and conducted hydrothermal treatment at 180 °C for 12 h. The hydrothermal process is able to make the sufficient reduction of GO to GR.[25,26,32] The precipitates thus obtained were centrifuged and washed with DI water until the pH of the supernatant was neutral and followed by a rinse of ethanol. After that, the sediments samples were dried at 60 °C in an electric oven.

2.2. Characterization. The phase composition of the samples were determined by a Bruker D8 Advance X-ray diffractometer (XRD) at 40 kV and 40 mA with Ni-filtered Cu Kα radiation in the 2θ range from 10° to 80° with a scan rate of 0.02° per second. UV–vis diffuse reflectance spectra (DRS) were recorded on a Cary-500 UV–vis–NIR spectrometer in which $BaSO_4$ powder was used as the internal standard. Nitrogen adsorption–desorption isotherms and the Brunauer–Emmett–Teller (BET) surface areas were collected at 77 K using Micromeritics ASAP2010 equipment. Transmission electron

microscopy (TEM) and high-resolution transmission electron microscopy (HRTEM) images were obtained using a JEOL model JEM 2010 EX instrument at an accelerating voltage of 200 kV. Photoelectrochemical measurements were performed in a homemade three electrode quartz cells with a PAR VMP3Multi potentiostat apparatus. Pt plate was used as the counter electrode, and the Ag/AgCl electrode was used as the reference electrode, while the working electrode was prepared on indium−tin oxide (ITO) conductor glass. The sample powder (10 mg) was ultrasonicated in 1 mL of anhydrous ethanol to disperse it evenly to get slurry. The slurry was spread onto ITO glass whose side part was previously protected using Scotch tape. The working electrode was dried overnight under ambient conditions. A copper wire was connected to the side part of the working electrode using a conductive tape. Uncoated parts of the electrode were isolated with epoxy resin. The electrolyte was 0.2 M of aqueous Na_2SO_4 solution (pH = 6.8) without additive. The visible light irradiation source was a 300 W Xe arc lamp system equipped with a UV cutoff filter ($\lambda > 400$ nm).

2.3. Catalyst Activity. The photocatalytic selective oxidation of benzyl alcohol was performed in a 10 mL Pyrex glass bottle that contained a mixture of alcohol (0.1 mmol) and 8 mg catalyst was dissolved in the solvent of benzotrifluoride (BTF) (1.5 mL).[32,33,36,64−68] The BTF was saturated with pure molecular oxygen. The reason for choosing BTF as solvent is because of its inertness to oxidation and high solubility for molecular oxygen.[69,70] The Pyrex glass bottle was filled with molecular oxygen at a pressure of 0.1 MPa and stirred for half an hour to make the catalyst blend evenly in the solution. Then, the suspensions were irradiated with a 300 W Xe arc lamp (PLS-SXE 300C, Beijing Perfectlight Co., Ltd.) with a UV-CUT filter to cut off light of wavelength < 400 nm. After the reaction, the mixture was centrifuged at 12000 rmp for 10 min to remove the catalyst particles thoroughly. The supernatant was analyzed with an Agilent Gas Chromatograph (GC-7820 fitted with a capillary FFAP analysis column). Controlled photoactivity experiments using different radical scavengers (*tert*-butyl alcohol as scavenger for hydroxyl radicals,[71,72] ammonium oxalate as scavenger for photogenerated holes,[73] silver nitrate as scavenger for electrons,[74,75] and benzoquinone as scavenger for superoxide radical species[72,76]) were performed similar to the above photocatalytic oxidation of benzyl alcohol except that the radical scavengers (0.1 mmol) were added to the reaction system. Conversion of alcohol, yield of aldehyde, and selectivity for aldehyde were defined as follows.

$$\text{conversion } (\%) = [(C_0 - C_{\text{alcohol}})/C_0] \times 100$$

$$\text{yield } (\%) = C_{\text{aldehyde}}/C_0 \times 100$$

$$\text{selectivity } (\%) = [C_{\text{aldehyde}}/(C_0 - C_{\text{alcohol}})] \times 100$$

Where, C_0 is the initial concentration of alcohol, and C_{alcohol} and C_{aldehyde} are the concentration of benzyl alcohol and benzaldehyde at a certain time after the photocatalytic reaction, respectively.

3. RESULTS AND DISCUSSION

The XRD patterns of the as-prepared TiO_2−carbon composites are shown in Figure 1. It is obvious that all of the TiO_2−carbon nanocomposites including TiO_2−GR nanocomposites and their analogues TiO_2−CNT and TiO_2−C_{60}, exhibit similar XRD patterns. The diffraction peaks for all samples match well with the anatase TiO_2 (JCPDS No. 21-1272). There are just some slight differences in the XRD patterns with the different carbon material. In comparison with the standard card of anatase TiO_2, it is easy to see that the kind of carbon materials and their weight addition ratio in the TiO_2−carbon nanocomposites have no obvious influence on the characteristic peaks of TiO_2. In Figure 1a and b, it can be found that no typical diffraction peaks of GR and CNT are observed in the corresponding nanocomposites, which can be ascribed to two reasons. On

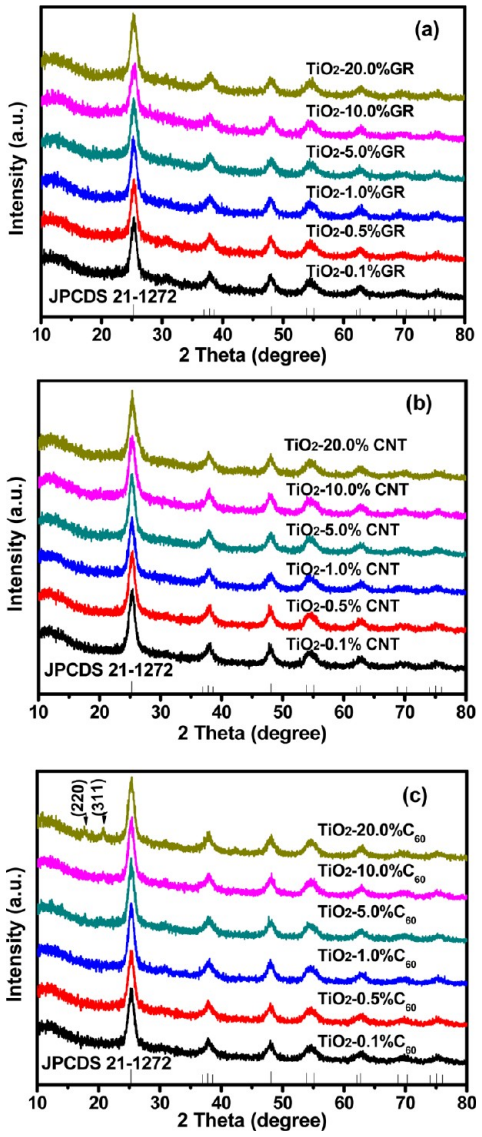

Figure 1. XRD patterns of TiO_2−GR nanocomposites (a) and their analogues TiO_2−CNT (b) and TiO_2−C_{60} nanocomposites (c).

the one hand, the weight addition ratios of carbon materials in the nanocomposites are relatively low. On the other hand, the main characteristic peaks of GR at 25.0° and CNT at 26.2° are probably shadowed by the (101) peak at 25.3° of anatase TiO_2, which is consistent with the previous reports.[26,32] As shown in Figure 1c, when the weight addition ratio of C_{60} is low in the nanocomposites, there is no obvious diffraction peaks of C_{60} and the XRD patterns are similar with the analogues GR−TiO_2 and TiO_2−CNT nanocomposites. However, as the weight addition ratios of C_{60} reach 20%, apparently, two new peaks located at 17.7° and 20.8° are present which can be indexed to the (220) and (311) crystal planes of Buckminster fullerene.[49,77]

Figure 2 displays the UV−vis diffuse reflectance spectra (DRS) of the as-obtained TiO_2−carbon nanocomposites. It can be seen clearly that the addition of GR, CNT, or C_{60} all induce the significant increased light absorption intensity in the visible light region. The continuous absorption band in the range of 400−800 nm is caused by the addition of carbon materials. Though the change of the kind of carbon material affects the shape of the absorption curve, which results from the

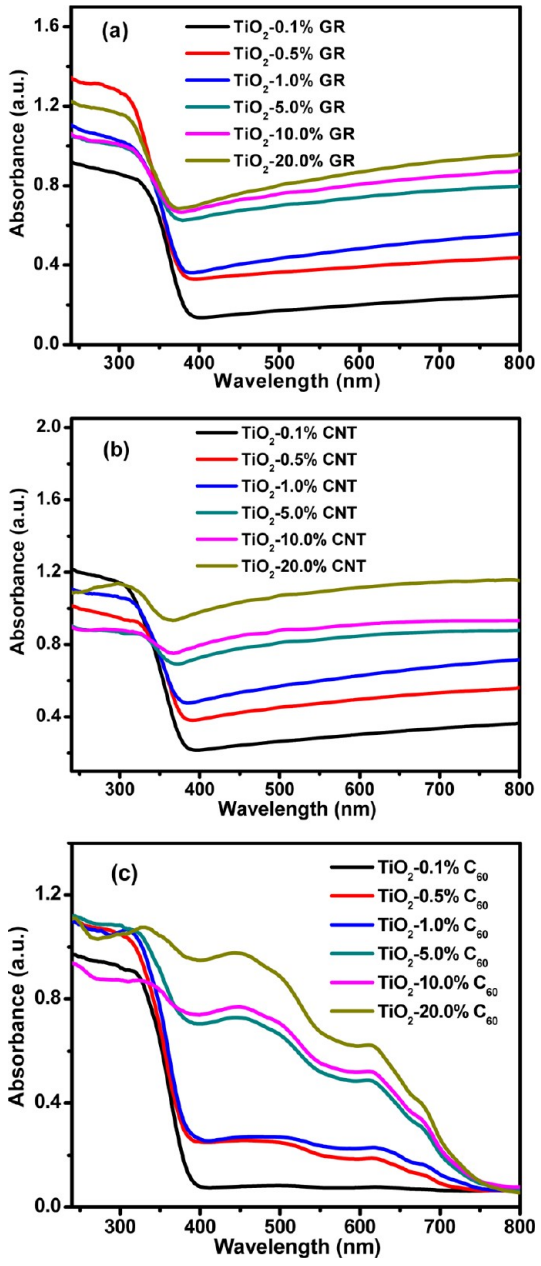

Figure 2. UV–vis diffuse reflectance spectra of TiO_2–GR nanocomposites (a) and their analogues TiO_2–CNT (b) and TiO_2–C_{60} nanocomposites (c).

dissimilarity in the natural optical properties of different carbon materials as reflected in the DRS of GR, CNT, and C_{60} (Supporting Information Figure S1), the rhythmicity stays the same. For all the carbon materials, the light absorption intensity in the visible light region increases accompanied with the augment of the addition amount of carbon materials. Furthermore, a qualitative red shift to higher wavelength is observed in the absorption edge of all TiO_2–GR, TiO_2–CNT, and TiO_2–C_{60} nanocomposites, which can be attributed to electronic interactions between GR, CNT, or C_{60} and TiO_2.[26,48,78] Such an extended optical absorption has also been observed in previous research works regarding GR–, CNT–, and C_{60}–semiconductor nanocomposites.[26,28,32,47−50] Therefore, the introduction of GR, CNT, or C_{60} into the matrix of TiO_2 is able to promote the visible light response of the nanocomposites of TiO_2–GR, TiO_2–CNT, and TiO_2–C_{60} effectively.

To understand the difference of GR, CNT, and C_{60} on enhancing the photocatalytic activity of TiO_2, we choose photocatalytic selective oxidation of benzyl alcohol to benzaldehyde as a model reaction.[32] Taking a view of the results as summarized in Figure 3a–c, we can see that, for the three different series of TiO_2–carbon nanocomposites, the optimum ingredient ratios of TiO_2–carbon always exist and differ in the kind of carbon materials. According to their photocatalytic performance for selective oxidation of benzyl alcohol to benzaldehyde under visible light irradiation, for TiO_2–GR, TiO_2–CNT, and TiO_2–C_{60}, the optimum nanocomposites are TiO_2–0.1% GR, TiO_2–0.5% CNT, and TiO_2–1.0% C_{60}, respectively. For these three optimum nanocomposites, the conversions of benzyl alcohol are all close to each other (ca. 40%), along with the selectivity higher than 95%. The photocatalytic selective oxidation of benzyl alcohol over the optimized nanocomposites as a function of time under visible light irradiation are also shown in Figure 3d–f. It is found that, for TiO_2–0.1% GR, TiO_2–0.5% CNT, and TiO_2–1.0% C_{60} nanocomposites, there is no significant difference in the conversion of benzyl alcohol and the selectivity for benzaldehyde along with the reaction time of 2, 4, 6, and 8 h. The similar phenomenon is also observed for selective oxidation of other substituted benzylic alcohols, i.e. no significant difference of photocatalytic performance among these three optimum TiO_2–carbon composite photocatalysts under visible light irradiation (Supporting Information Figure S2). In addition, it should be noted that the photoactivity of optimum TiO_2–0.1% GR and TiO_2–0.5% CNT is higher than the optimum TiO_2–5% GR and TiO_2–5% CNT that were prepared from the hydrolysis of TiF_4 along with hydrothermal post-treatment process.[32] In the previous work of our group, the photocatalyst of TiO_2–GR with intimate interfacial contact between GR and TiO_2 exhibits significantly enhanced photocatalytic activities as compared to TiO_2–CNT with poor interfacial contact. It has been proved that the interfacial contact between carbon and semiconductor is an important factor, which affects the photocatalytic activities of the carbon–semiconductor composite photocatalysts.[32] Thus, in order to obtain a relatively objective and rational comparison among the three different carbon materials on affecting the photoactivity of semiconductor, similar interfacial contact should be considered. In the present work, by employing the combination of sol–gel and hydrothermal method, we have prepared a series of TiO_2–GR, TiO_2–CNT, and TiO_2–C_{60} nanocomposites with different weight addition ratios of carbon contents, which all have a good interfacial contact, ensuring that the comparison study among GR, CNT, and C_{60} is performed in a reasonable framework. In addition, as compared with our previous report, the obvious difference in photoactivity clearly implies that the preparation methods play a significant effect on the synergetic interaction between semiconductor TiO_2 and carbon contents and, thus, different photocatalytic performance.[25,32]

To further obtain the microscopic structure information of the carbon–TiO_2 nanocomposites and study the influence of the carbon materials on TiO_2 morphology, transmission electron microscopy (TEM) analysis has been carried out, as displayed in Figure 4. It can be seen from Figure 4a and b that GR nanosheets and carbon nanotubes are covered with TiO_2 nanoparticles. The energy dispersive X-ray spectrum (EDX) was employed to prove the existence of GR in TiO_2–0.1% GR.

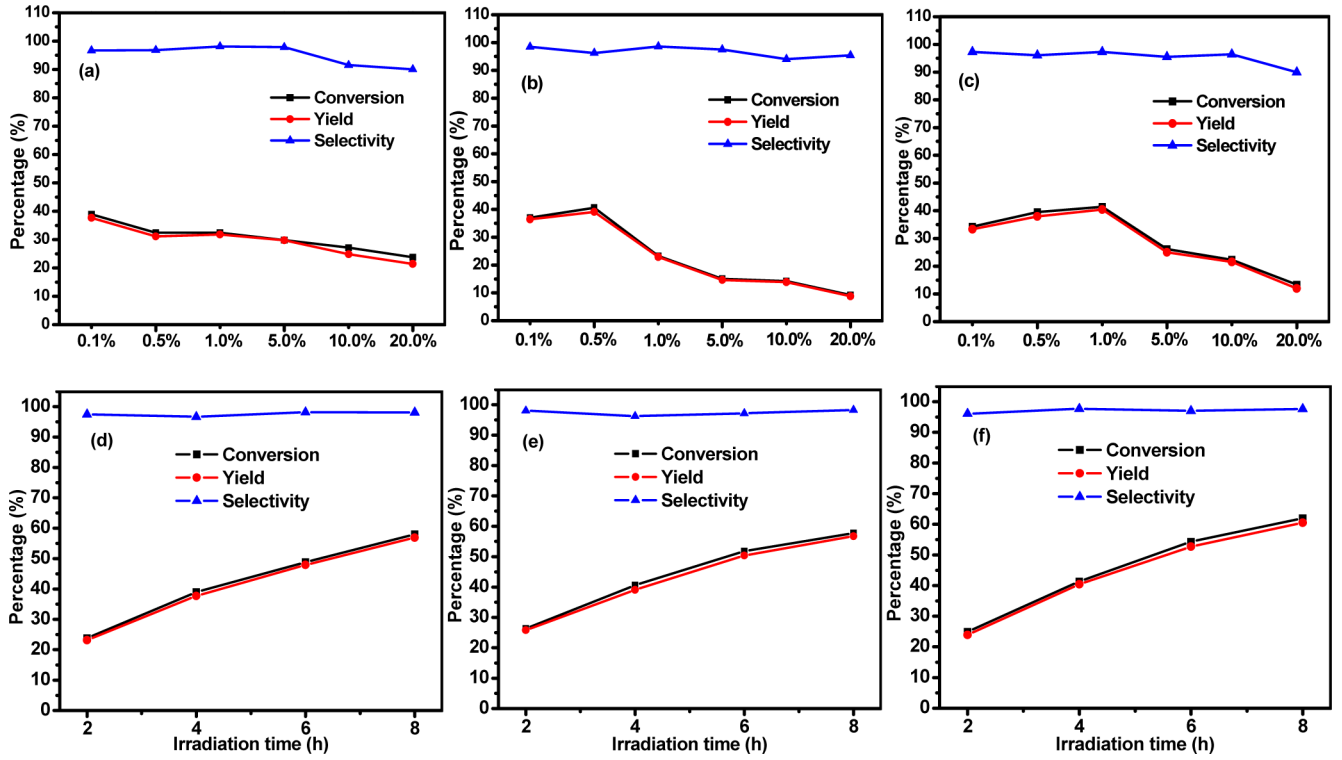

Figure 3. Selective oxidation of benzyl alcohol to benzaldehyde over the nanocomposites of TiO_2–GR (a), TiO_2–CNT (b), and TiO_2–C_{60} (c) with different weight addition ratios of GR, CNT, and C_{60}, respectively, under visible light irradiation of 4 h; time-online profiles of conversion, yield, and selectivity over the optimal TiO_2–0.1% GR (d), TiO_2–0.5% CNT (e), and TiO_2–1.0% C_{60} (f) nanocomposites.

As displayed in Figure S3 (Supporting Information), the result of EDX gives the signals of C, O, Cu, and Ti elements. Because the lacey support film without carbon coating is used, the signal of C must come from the GR sheet in the nanocomposites, which confirms the composition of the sample. As for TiO_2–C_{60} nanocomposites, it is easy to observe from Figure 4c that a coverture layer with amorphous structure covers the surface of the TiO_2 nanoparticles. The thickness of the coverture layer was estimated to be 1 nm, close to the size of the C_{60} molecule (0.71 nm).[79] Therefore, it can be estimated that the outer layer is C_{60}, which is dispersed on the surface of TiO_2 with a monolayer structure and this is in accordance with the previous wok.[47,49] Watching all the TEM images, we can see that there is no obvious influence of carbon addition on the morphology and particle size of TiO_2 nanoparticles, regardless of what kinds of carbon ingredients was used to combine with TiO_2. For the three optimal ingredient ratios, TiO_2 all displays the similar morphology; the particle shape and the size of the TiO_2 nanoparticles in TiO_2–carbon composites are all about 10 nm. The selected area electron diffraction (SAED) patterns as displayed in the insets of Figure 4 indicate that the TiO_2 in the nanocomposites possesses the polycrystalline structure, in agreement with the result of XRD analysis. In addition, from the TEM analysis, it can be seen that the carbon ingredients and TiO_2 have a good interfacial contact for the composites of TiO_2–0.1% GR, TiO_2–0.5% CNT, and TiO_2–1.0% C_{60}.

It is known that the lifetime of photogenerated electron–hole pairs is a key factor determining the photocatalytic activity of carbon–semiconductor nanocomposites.[80,81] Since the good interfacial contact between the carbon materials and TiO_2 is observed, is there significant difference in the roles of fullerene, carbon nanotube, and graphene on lengthening the lifetime of photogenerated electron–hole pairs? To address the above issue, the transient photocurrent responses of TiO_2–0.1% GR, TiO_2–0.5% CNT, and TiO_2–1.0% C_{60} have been investigated under intermittent visible light illumination with the wavelength range used in the photocatalytic reactions, and the results are showed in Figure 5. Because it is well-known that TiO_2 has negligible photocurrent under visible light irradiation,[32] it is easy to observe that the addition of different carbon ingredients all can enhance the photocurrent significantly for TiO_2–carbon photocatalysts under visible light irradiation and the photocurrent rapidly decreases to zero as long as the light is switched off. The photocurrent is formed mainly by the diffusion of the photogenerated electrons to the back contact, and meanwhile, the photoinduced holes are taken up by the hole acceptor in the electrolyte.[82] Therefore, the enhanced photocurrent over TiO_2–carbon nanocomposites indicates a more efficient separation of the photoexcited electron–hole pairs and longer lifetime of the photogenerated charge carriers. Moreover, no obvious photocurrent decay is observed. This indicates that the transport of photogenerated electrons to carbon materials is markedly effective. The adjacent and stable photocurrent of TiO_2–0.1% GR, TiO_2–0.5% CNT, and TiO_2–1.0% C_{60} nanocomposites highlight the similar role of GR, CNT, and C_{60} in prolonging the lifetime of photogenerated electron–hole pairs. More importantly, there is no significant difference on the ability of three carbon materials on lengthening the lifetime of photogenerated electron–hole pairs of TiO_2–carbon nanocomposites.

In addition, electrochemical impedance spectroscopy (EIS) Nyquist plots have also been carried out. As shown in Figure 6, the Nyquist plots of TiO_2–0.1% GR, TiO_2–0.5% CNT, and TiO_2–1.0% C_{60} nanocomposites electrode materials cycled in 0.2 M Na_2SO_4 electrolyte solution all show semicycles at high frequencies. Since the preparation of the electrodes and

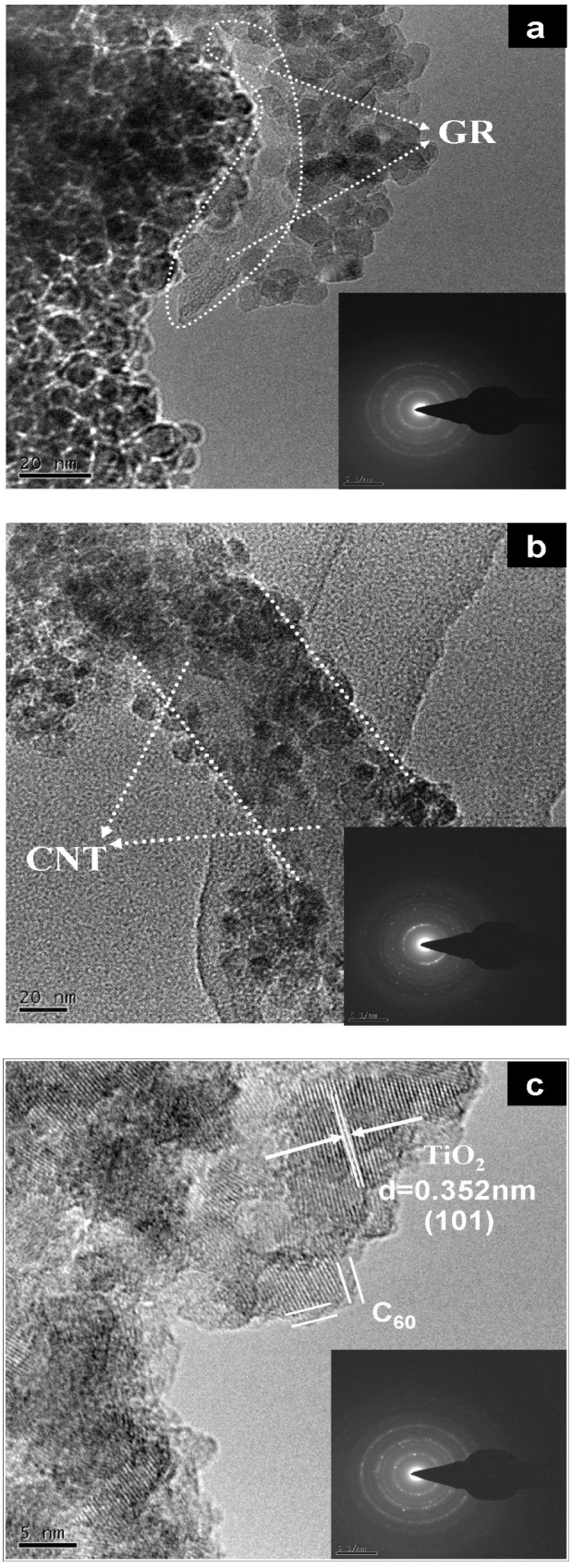

Figure 4. TEM images of TiO_2−0.1% GR (a), TiO_2−0.5% CNT (b), and TiO_2−1.0% C_{60} (c).

electrolyte used are alike, the high-frequency semicircles are related to the resistance of the electrodes.[83] In electrochemical

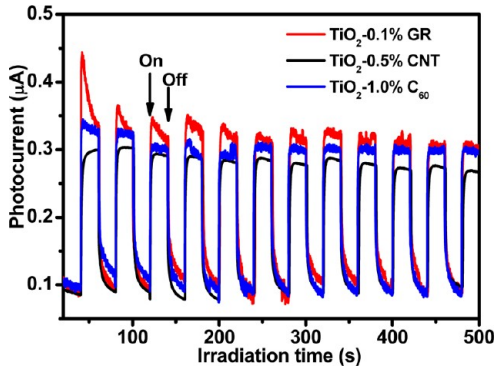

Figure 5. Transient photocurrent response of TiO_2−0.1% GR, TiO_2−0.5% CNT, and TiO_2−1.0% C_{60} nanocomposites in 0.2 M Na_2SO_4 aqueous solution without bias versus Ag/AgCl under the irradiation of visible light.

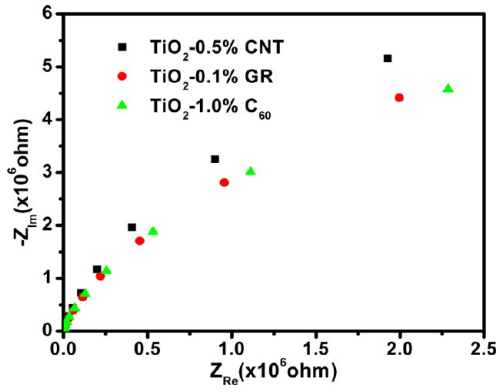

Figure 6. Electrochemical impedance spectroscopy (EIS) Nyquist plots of TiO_2−0.1% GR, TiO_2−0.5% CNT, and TiO_2−1.0% C_{60} nanocomposites.

spectra, the high-frequency arc corresponds to the charge transfer limiting process and can be attributed to the double-layer capacitance in parallel with the charge transfer resistance at the contact interface between electrode and electrolyte solution.[84] It can be seen from Figure 6 that the change of carbon materials leads to little difference in the EIS Nyquist plots; on the other hand, the charge transfer resistance can be directly measured as the semicircle diameter. So, the nearly overlapped plots of TiO_2−0.1% GR and TiO_2−1.0% C_{60} mean a similar separation of photogenerated electron-hole pairs, and the interfacial charge transfer to the electron donor/electron acceptor of them are a bit faster than TiO_2−0.5% CNT nanocomposites, which is consistent with the results of photocurrent test.

In order to explore the influence of GR, CNT, and C_{60} on surface area and porosity of TiO_2−carbon nanocomposites, and thus understand the effect of different carbon materials on the photocatalytic performance, the surface area and porosity of TiO_2−0.1% GR, TiO_2−0.5% CNT, and TiO_2−1.0% C_{60} have been investigated, as displayed in Figure 7. According to the IUPAC classification,[85] it can be seen that all these three nanocomposites display a type IV isotherm with a typical H3 hysteresis loop characteristic of mesoporous solids, which is confirmed by the corresponding pore size distribution as shown in the inset of Figure 7. The similar shapes of their hysteresis loops also indicate the similar pore shapes. The specific Brunauer−Emmett−Teller (BET) surface area and pore

dx.doi.org/10.1021/am3029798 | ACS Appl. Mater. Interfaces 2013, 5, 1156−1164

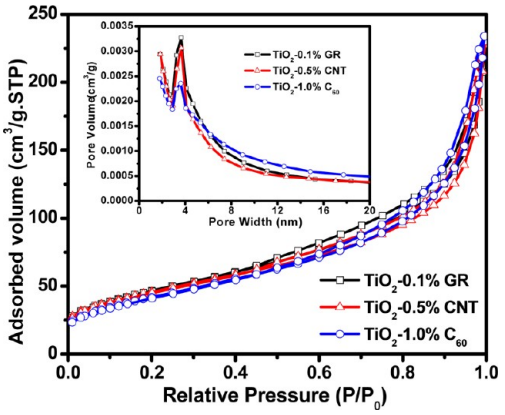

Figure 7. BET adsorption−desorption isotherm of TiO_2−0.1% GR, TiO_2−0.5% CNT, and TiO_2−1.0% C_{60} nanocomposites. (inset) Corresponding pore size distribution.

volume are 174 m^2/g and 0.35 cm^3/g for TiO_2−0.1% GR, 166 m^2/g and 0.35 cm^3/g for TiO_2−0.5% CNT, 165 m^2/g, 0.36 cm^3/g for TiO_2−1.0% C_{60}. It is clear that they are very close to each other. This is reasonable because, with such a small amount doping of carbon, the surface area and porosity are mainly dominated by TiO_2 ingredients. In addition, adsorption experiments in the dark for benzyl alcohol also have been performed. As displayed in Figure 8, the results suggest that

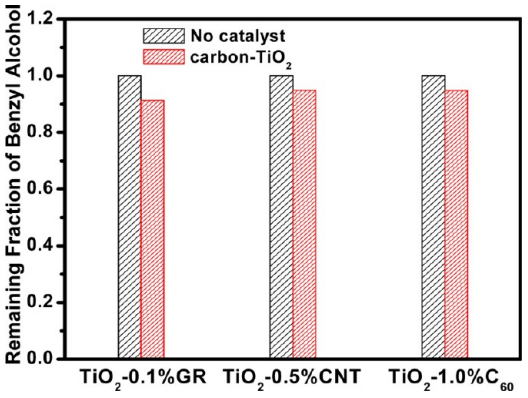

Figure 8. Remaining fraction of benzyl alcohol after the adsorption−desorption equilibrium is achieved over TiO_2−0.1% GR, TiO_2−0.5% CNT, and TiO_2−1.0% C_{60} nanocomposites.

there is no obvious difference of adsorptivity among the three different TiO_2−carbon nanocomposites, and this case is also observed for other benzylic alcohols (Supporting Information Figure S4).

To further understand the underlying reaction mechanism for the photocatalytic selective oxidation of benzyl alcohol over the as-prepared TiO_2−carbon photocatalysts, a series of controlled experiments with addition of different scavengers for the photogenerated radical species have been imposed on the oxidation process.[71] As shown in Figure 9, when the trapping agent of *tert*-butyl alcohol (TBA) as the radical scavenger for hydroxyl radicals (·OH) is added to the BTF dispersions of the three optimum nanocomposites,[71,72] compared with the original experiments without the radical scavengers, there is almost no change on the conversion of benzyl alcohol. This observation is reasonable because, in the BTF solvent, no ·OH radicals are formed.[32,33,65−67,71] When the quencher of ammonium oxalate (AO) for holes (h^+) is

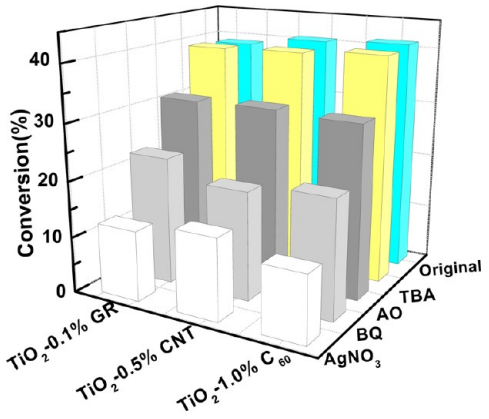

Figure 9. Controlled experiments using different radical scavengers for the photocatalytic selective oxidation of benzyl alcohol over TiO_2−carbon nanocomposites in the BTF solvent: reaction with *tert*-butyl alcohol (TBA) as the radical scavenger for hydroxyl radicals, reaction with ammonium oxalate (AO) as scavenger for photogenerated holes, reaction with benzoquinone (BQ) as scavenger for superoxide radicals, and reaction with $AgNO_3$ as scavenger for photogenerated electrons under visible light irradiation for 4 h.

added into the reaction system,[71,73] although the conversion of benzyl alcohol has a measurable decrease, a moderate conversion of benzyl alcohol can still be achieved. The photocatalytic conversion almost falls by half when the radical scavenger, benzoquinone (BQ), for superoxide radical species ($O_2{\cdot}^-$) is added into the reaction system.[71,72,76] Besides, the controlled experiment, using $AgNO_3$ as the radical scavenger for electrons (e^-),[71,74,75] shows that the conversion of benzyl alcohol is significantly declined to about 10%. These results clearly suggest that the photocatalytic selective oxidation of benzyl alcohol to benzaldehyde over the as-prepared TiO_2−carbon photocatalysts is intimate with the photogenerated electron−hole pairs and the superoxide radical species ($O_2{\cdot}^-$). In other words, photogenerated holes, electrons, and superoxide radicals are the primary active species for photocatalytic selective oxidation of benzyl alcohol. In addition, it should be noted that the photocatalytic experiments are performed under oxygen-saturated condition and the present molecular oxygen (O_2) can act as electron-acceptors by which oxygen is activated and the recombination of electron−hole pairs is inhibited.[71,86] Summing up the above discussion, we can propose for the series of TiO_2−carbon (GR, CNT, and C_{60}) photocatalysts that they follow the analogous tentative reaction mechanism toward selective oxidation of benzyl alcohol in the BTF solvent under visible light irradiation.

The present work suggests that the photocatalytic performance of TiO_2−carbon is significantly affected by the preparation methods. The difference in preparation methods causes the different structural composition and synergetic interaction between TiO_2 and carbon, which thus influences the photocatalytic performance of TiO_2−carbon composites. Thus, although GR is more popular than its forebears (CNT and C_{60}) at present with regard to synthesis and application of semiconductor−carbon composite photocatalysts, it is still too early to draw a definitely decisive answer for GR's unique superiority to other carbon allotropes on improving the photocatalytic performance of semiconductor. More efforts should be keenly required to understand the role and mechanism of GR on affecting the photocatalytic properties

of GR−semiconductor composite photocatalysts, instead of joining the GR gold rush.[25]

CONCLUSIONS

In summary, we have prepared a series of TiO_2−carbon (GR, CNT, and C_{60}) nanocomposites with different weight addition ratios of carbon materials by a sol−gel process along with hydrothermal post-treatment. By using the photocatalytic oxidation of benzyl alcohol to benzaldehyde as a testing reaction, we have investigated the photocatalytic performance of the synthesized TiO_2−carbon composites. The results have demonstrated that for the TiO_2−GR, TiO_2−CNT, and TiO_2−C_{60} nanocomposites, the optimal ingredient ratios exist at low weight additions, and their photoactivities are rather similar. The photocatalytic selective oxidation of benzyl alcohol over the TiO_2−carbon nanocomposites with different carbon materials follows the analogous reaction mechanism. In addition, the introduction of carbon materials makes little difference in the crystal phase, particle size, surface area, pore volume, and the morphology of TiO_2. The addition of GR, CNT, and C_{60} all can induce the increased light absorption intensity in visible light region and promote the visible light response of the nanocomposites of TiO_2−GR, TiO_2−CNT, and TiO_2−C_{60} effectively; they can also promote an efficient separation of the photoexcited electron−hole pairs in a similar way. Thus, we do not observe the significant difference of GR on improving the photoactivity of TiO_2 as compared to CNT and C_{60}. It is hoped that this work could promote the more objective understanding on the analogy and difference of these three carbon allotropes on the rational synthesis and photoactivity improvement of semiconductor−carbon composites for target applications in heterogeneous photocatalysis. Research in this respect would significantly advance how the remarkable properties of GR could best be utilized to design the unique, more efficient GR-based composite photocatalysts for specific applications.

ASSOCIATED CONTENT

Supporting Information

UV−vis diffuse reflectance spectra of GR, CNT, and C_{60}, selective oxidation of substituted benzylic alcohols to aldehydes over the optimal TiO_2−0.1% GR, TiO_2−0.5% CNT, and TiO_2−1.0% C_{60} nanocomposites under the irradiation of visible light; energy dispersive X-ray (EDX) image of the TiO_2−0.1% GR nanocomposite; remaining fraction of substituted benzylic alcohols after the adsorption−desorption equilibrium is achieved over TiO_2−0.1% GR, TiO_2−0.5% CNT, and TiO_2−1.0% C_{60} nanocomposites. This material is available free of charge via the Internet at http://pubs.acs.org.

AUTHOR INFORMATION

Corresponding Author

*Tel./fax: +86 591 83779326. E-mail: yjxu@fzu.edu.cn.

Notes

The authors declare no competing financial interest.

ACKNOWLEDGMENTS

The support by the National Natural Science Foundation of China (NSFC) (21173045, 20903023), the Award Program for Minjiang Scholar Professorship, the Natural Science Foundation of Fujian Province for Distinguished Investigator Grant (2012J06003), Program for Changjiang Scholars and Innovative Research Team in Universities (PCSIRT0818), Program for Returned High-Level Overseas Chinese Scholars of Fujian Province, and the Project Sponsored by the Scientific Research Foundation for the Returned Overseas Chinese Scholars, State Education Ministry, is gratefully acknowledged.

REFERENCES

(1) Novoselov, K. S.; Geim, A. K.; Morozov, S. V.; Jiang, D.; Zhang, Y.; Dubonos, S. V.; Grigorieva, I. V.; Firsov, A. A. *Science* **2004**, *306*, 666−669.
(2) Bolotin, K. I.; Sikes, K. J.; Jiang, Z.; Klima, M.; Fudenberg, G.; Hone, J.; Kim, P.; Stormer, H. L. *Solid State Commun.* **2008**, *146*, 351−355.
(3) Morozov, S. V.; Novoselov, K. S.; Katsnelson, M. I.; Schedin, F.; Elias, D. C.; Jaszczak, J. A.; Geim, A. K. *Phys. Rev. Lett.* **2008**, *100*, 016602.
(4) Stoller, M. D.; Park, S.; Zhu, Y.; An, J.; Ruoff, R. S. *Nano Lett.* **2008**, *8*, 3498−3502.
(5) Balandin, A. A.; Ghosh, S.; Bao, W.; Calizo, I.; Teweldebrhan, D.; Miao, F.; Lau, C. N. *Nano Lett.* **2008**, *8*, 902−907.
(6) Li, X.; Zhu, Y.; Cai, W.; Borysiak, M.; Han, B.; Chen, D.; Piner, R. D.; Colombo, L.; Ruoff, R. S. *Nano Lett.* **2009**, *9*, 4359−4363.
(7) Geim, A. K.; Novoselov, K. S. *Nat. Mater.* **2007**, *6*, 183−191.
(8) Katsnelson, M. I.; Novoselov, K. S. *Solid State Commun.* **2007**, *143*, 3−13.
(9) Geim, A. K. *Science* **2009**, *324*, 1530−1534.
(10) Allen, M. J.; Tung, V. C.; Kaner, R. B. *Chem. Rev.* **2009**, *110*, 132−145.
(11) Rao, C. N. R.; Sood, A. K.; Subrahmanyam, K. S.; Govindaraj, A. *Angew. Chem., Int. Ed.* **2009**, *48*, 7752−7777.
(12) Guo, S.; Dong, S. *Chem. Soc. Rev.* **2011**, *40*, 2644−2672.
(13) Bai, H.; Li, C.; Shi, G. *Adv. Mater.* **2011**, *23*, 1089−1115.
(14) Kamat, P. V. *J. Phys. Chem. Lett.* **2009**, *1*, 520−527.
(15) Stankovich, S.; Dikin, D. A.; Dommett, G. H. B.; Kohlhaas, K. M.; Zimney, E. J.; Stach, E. A.; Piner, R. D.; Nguyen, S. T.; Ruoff, R. S. *Nature* **2006**, *442*, 282−286.
(16) Li, X.; Wang, X.; Zhang, L.; Lee, S.; Dai, H. *Science* **2008**, *319*, 1229−1232.
(17) Compton, O. C.; Nguyen, S. T. *Small* **2010**, *6*, 711−723.
(18) Wang, X.; Zhi, L.; Mullen, K. *Nano Lett.* **2007**, *8*, 323−327.
(19) Machado, B. F.; Serp, P. *Catal. Sci. Technol.* **2012**, *2*, 54−75.
(20) An, X.; Yu, J. C. *RSC Adv.* **2011**, *1*, 1426−1434.
(21) Xiang, Q.; Yu, J.; Jaroniec, M. *Chem. Soc. Rev.* **2012**, *41*, 782−796.
(22) Liang, Y. T.; Hersam, M. C. *J. Am. Chem. Soc.* **2010**, *132*, 17661−17663.
(23) Ng, Y. H.; Lightcap, I. V.; Goodwin, K.; Matsumura, M.; Kamat, P. V. *J. Phys. Chem. Lett.* **2010**, *1*, 2222−2227.
(24) Bell, N. J.; Ng, Y. H.; Du, A.; Coster, H.; Smith, S. C.; Amal, R. *J. Phys. Chem. C* **2011**, *115*, 6004−6009.
(25) Zhang, N.; Zhang, Y.; Xu, Y.-J. *Nanoscale.* **2012**, *4*, 5792−5813.
(26) Zhang, Y.; Tang, Z.-R.; Fu, X.; Xu, Y.-J. *ACS Nano* **2010**, *4*, 7303−7314.
(27) Chen, C.; Cai, W.; Long, M.; Zhou, B.; Wu, Y.; Wu, D.; Feng, Y. *ACS Nano* **2010**, *4*, 6425−6432.
(28) Zhao, D.; Sheng, G.; Chen, C.; Wang, X. *Appl. Catal., B* **2012**, *111−112*, 303−308.
(29) Zhang, J.; Xiong, Z.; Zhao, X. S. *J. Mater. Chem.* **2011**, *21*, 3634−3640.
(30) Akhavan, O.; Ghaderi, E. *J. Phys. Chem. C* **2009**, *113*, 20214−20220.
(31) Ai, Z.; Ho, W.; Lee, S. *J. Phys. Chem. C* **2011**, *115*, 25330−25337.
(32) Zhang, Y.; Tang, Z.-R.; Fu, X.; Xu, Y.-J. *ACS Nano* **2011**, *5*, 7426−7435.
(33) Zhang, N.; Zhang, Y.; Pan, X.; Fu, X.; Liu, S.; Xu, Y.-J. *J. Phys. Chem. C* **2011**, *115*, 23501−23511.

(34) Li, X.-H.; Chen, J.-S.; Wang, X.; Sun, J.; Antonietti, M. *J. Am. Chem. Soc.* **2011**, *133*, 8074−8077.
(35) Liang, Y. T.; Vijayan, B. K.; Gray, K. A.; Hersam, M. C. *Nano Lett.* **2011**, *11*, 2865−2870.
(36) Zhang, N.; Zhang, Y.; Pan, X.; Yang, M.-Q.; Xu, Y.-J. *J. Phys. Chem. C* **2012**, *116*, 18023−18031.
(37) Jia, L.; Wang, D.-H.; Huang, Y.-X.; Xu, A.-W.; Yu, H.-Q. *J. Phys. Chem. C* **2011**, *115*, 11466−11473.
(38) Xiang, Q.; Yu, J.; Jaroniec, M. *J. Am. Chem. Soc.* **2012**, *134*, 6575−6578.
(39) Ye, A.; Fan, W.; Zhang, Q.; Deng, W.; Wang, Y. *Catal. Sci. Technol.* **2012**, *2*, 969−978.
(40) Mukherji, A.; Seger, B.; Lu, G. Q.; Wang, L. *ACS Nano* **2011**, *5*, 3483−3492.
(41) Iwase, A.; Ng, Y. H.; Ishiguro, Y.; Kudo, A.; Amal, R. *J. Am. Chem. Soc.* **2011**, *133*, 11054−11057.
(42) Ng, Y. H.; Iwase, A.; Kudo, A.; Amal, R. *J. Phys. Chem. Lett.* **2010**, *1*, 2607−2612.
(43) Fan, W.; Lai, Q.; Zhang, Q.; Wang, Y. *J. Phys. Chem. C* **2011**, *115*, 10694−10701.
(44) Fan, W.; Zhang, Q.; Wang, Y. *Phys. Chem. Chem. Phys.* **2012**, DOI: 10.1039/C2CP43524A.
(45) Kroto, H. W.; Heath, J. R.; O'Brien, S. C.; Curl, R. F.; Smalley, R. E. *Nature* **1985**, *318*, 162−163.
(46) Iijima, S. *Nature* **1991**, *354*, 56−58.
(47) Zhu, S.; Xu, T.; Fu, H.; Zhao, J.; Zhu, Y. *Environ. Sci. Technol.* **2007**, *41*, 6234−6239.
(48) Fu, H.; Xu, T.; Zhu, S.; Zhu, Y. *Environ. Sci. Technol.* **2008**, *42*, 8064−8069.
(49) Yu, J.; Ma, T.; Liu, G.; Cheng, B. *Dalton Trans.* **2011**, *40*, 6635−6644.
(50) Xu, Y.-J.; Zhuang, Y.; Fu, X. *J. Phys. Chem. C* **2010**, *114*, 2669−2676.
(51) Lin, J.; Zong, R.; Zhou, M.; Zhu, Y. *Appl. Catal., B* **2009**, *89*, 425−431.
(52) Tang, Z.-R.; Li, F.; Zhang, Y.; Fu, X.; Xu, Y.-J. *J. Phys. Chem. C* **2011**, *115*, 7880−7886.
(53) Kim, Y. K.; Park, H. *Energy Environ. Sci.* **2011**, *4*, 685−694.
(54) Chen, W.; Fan, Z.; Zhang, B.; Ma, G.; Takanabe, K.; Zhang, X.; Lai, Z. *J. Am. Chem. Soc.* **2011**, *133*, 14896−14899.
(55) Peng, T.; Zeng, P.; Ke, D.; Liu, X.; Zhang, X. *Energy Fuels* **2011**, *25*, 2203−2210.
(56) Yu, J.; Yang, B.; Cheng, B. *Nanoscale* **2012**, *4*, 2670−2677.
(57) Liang, Y. T.; Vijayan, B. K.; Lyandres, O.; Gray, K. A.; Hersam, M. C. *J. Phys. Chem. Lett.* **2012**, *3*, 1760−1765.
(58) Kamat, P. V.; Gevaert, M.; Vinodgopal, K. *J. Phys. Chem. B* **1997**, *101*, 4422−4427.
(59) Eder, D.; Windle, A. H. *J. Mater. Chem.* **2008**, *18*, 2036−2043.
(60) Meyer, J. C.; Geim, A. K.; Katsnelson, M. I.; Novoselov, K. S.; Booth, T. J.; Roth, S. *Nature* **2007**, *446*, 60−63.
(61) Wang, C.-C.; Ying, J. Y. *Chem. Mater.* **1999**, *11*, 3113−3120.
(62) Keshmiri, M.; Mohseni, M.; Troczynski, T. *Appl. Catal., B* **2004**, *53*, 209−219.
(63) Hummers, W. S.; Offeman, R. E. *J. Am. Chem. Soc.* **1958**, *80*, 1339−1339.
(64) Tang, Z.-R.; Zhang, Y.; Xu, Y.-J. *ACS Appl. Mater. Interfaces* **2012**, *4*, 1512−1520.
(65) Zhang, N.; Fu, X.; Xu, Y.-J. *J. Mater. Chem.* **2011**, *21*, 8152−8158.
(66) Zhang, N.; Liu, S.; Fu, X.; Xu, Y.-J. *J. Phys. Chem. C* **2011**, *115*, 22901−22909.
(67) Zhang, N.; Liu, S.; Fu, X.; Xu, Y.-J. *J. Mater. Chem.* **2012**, *22*, 5042−5052.
(68) Zhang, Y.; Zhang, N.; Tang, Z.-R.; Xu, Y.-J. *Phys. Chem. Chem. Phys.* **2012**, *14*, 9167−9175.
(69) Zhang, M.; Chen, C.; Ma, W.; Zhao, J. *Angew. Chem., Int. Ed.* **2008**, *47*, 9730−9733.
(70) Zhang, M.; Wang, Q.; Chen, C.; Zang, L.; Ma, W.; Zhao, J. *Angew. Chem., Int. Ed.* **2009**, *48*, 6081−6084.
(71) Zhang, Y.; Zhang, N.; Tang, Z.-R.; Xu, Y.-J. *Chem. Sci.* **2012**, *3*, 2812−2822.
(72) Raja, P.; Bozzi, A.; Mansilla, H.; Kiwi, J. *J. Photochem. Photobiol., A* **2005**, *169*, 271−278.
(73) Carp, O.; Huisman, C. L.; Reller, A. *Prog. Solid State Chem.* **2004**, *32*, 33−177.
(74) Liu, S.; Zhang, N.; Tang, Z.-R.; Xu, Y.-J. *ACS Appl. Mater. Interfaces* **2012**, *4*, 6378−6385.
(75) Primo, A.; Marino, T.; Corma, A.; Molinari, R.; García, H. *J. Am. Chem. Soc.* **2011**, *133*, 6930−6933.
(76) Stylidi, M.; Kondarides, D. I.; Verykios, X. E. *Appl. Catal., B* **2004**, *47*, 189−201.
(77) Apostolopoulou, V.; Vakros, J.; Kordulis, C.; Lycourghiotis, A. *Colloids Surf., A* **2009**, *349*, 189−194.
(78) Zhang, Y.; Zhang, N.; Tang, Z.-R.; Xu, Y.-J. *ACS Nano* **2012**, *6*, 9777−9789.
(79) Kratschmer, W.; Lamb, L. D.; Fostiropoulos, K.; Huffman, D. R. *Nature* **1990**, *347*, 354−358.
(80) Woan, K.; Pyrgiotakis, G.; Sigmund, W. *Adv. Mater.* **2009**, *21*, 2233−2239.
(81) Leary, R.; Westwood, A. *Carbon* **2011**, *49*, 741−772.
(82) Soedergren, S.; Hagfeldt, A.; Olsson, J.; Lindquist, S.-E. *J. Phys. Chem.* **1994**, *98*, 5552−5556.
(83) Wang, D.; Choi, D.; Li, J.; Yang, Z.; Nie, Z.; Kou, R.; Hu, D.; Wang, C.; Saraf, L. V.; Zhang, J.; Aksay, I. A.; Liu, J. *ACS Nano* **2009**, *3*, 907−914.
(84) Lu, T.; Zhang, Y.; Li, H.; Pan, L.; Li, Y.; Sun, Z. *Electrochim. Acta* **2010**, *55*, 4170−4173.
(85) Sing, K. S. W.; Everett, D. H.; Haul, R. A. W.; Moscou, L.; Pierotti, R. A.; Rouquerol, J.; Siemieniewska, T. *Pure Appl. Chem.* **1985**, *57*, 603−619.
(86) Maldotti, A.; Molinari, A.; Amadelli, R. *Chem. Rev.* **2002**, *102*, 3811−3836.